

# Brain region-specific vulnerability of astrocytes in response to 3-nitropropionic acid is mediated by cytochrome c oxidase isoform expression

Magdalena Misiak · Shilpee Singh · Sascha Drewlo · Cordian Beyer · Susanne Arnold

Received: 1 February 2010 / Accepted: 18 May 2010  
© Springer-Verlag 2010

**Abstract** Brain region specificity is a feature characteristic of neurodegenerative disorders, such as Huntington's disease (HD). We have studied the brain region-specific vulnerability of striatal compared with cortical and mesencephalic astrocytes treated with 3-nitropropionic acid (NPA), an in vitro model of HD. Mitochondrial dysfunction is involved in neurodegenerative processes. We have previously demonstrated a causal relationship between NPA-induced transcription of the cytochrome c oxidase (COX) subunit IV isoform (*cox4i2*) and increased oxidative stress leading to higher rates of necrotic cell death in striatal astrocytes by the application of a small interfering RNA knockdown system. Here, we have investigated the correlation of COX IV-2 protein expression with intracellular ATP content, mitochondrial peroxide production, and viability of astrocytes from three different brain regions. In cortical and mesencephalic astrocytes, NPA caused an elevation of *cox4i2* transcription as in striatal astroglia. However, increased COX IV-2 and decreased COX IV-1 protein expression levels have been observed only in striatal astrocytes. In agreement with our hypothesis, striatal astrocytes showed the highest levels of peroxide production and necrotic cell death rates compared with cortical and mesencephalic astroglia. Thus, we suggest that the higher vulnerability of astrocytes from the striatum in our in vitro model of HD is, at least in part, based on brain

region-specific differences of the COX IV-2/COX IV-1 protein ratios and accompanied elevated oxidative stress.

**Keywords** Striatum · Cortex · Mesencephalon · Mitochondria · Reactive oxygen species

## Introduction

Cytochrome c oxidase (COX) is located in the inner mitochondrial membrane catalyzing the electron transfer from ferrocyanochrome c to oxygen. Each monomer of the dimeric enzyme complex consists of three mitochondria-encoded catalytic and ten nucleus-encoded regulatory subunits (Tsukihara et al. 1996; Grossman and Lomax 1997). The nucleus-encoded COX subunit IV-1 plays a crucial role in regulating energy metabolism and oxidative stress (Arnold and Kadenbach 1999; Kadenbach et al. 2000, 2004; Horvat et al. 2006; Singh et al. 2009). At high intracellular energy levels, ATP binds to the N-terminus of COX subunit IV-1 and inhibits the enzyme activity allosterically (Arnold and Kadenbach 1997, 1999; Horvat et al. 2006). This regulatory mechanism enables the enzyme to detect the intracellular energy level and facilitates the adjustment of ATP production to cellular energy demand. This mechanism is conferred on the mammalian enzyme by the ubiquitously transcribed COX isoform IV-1, whereas a second isoform of COX subunit IV (COX IV-2) impedes this regulatory mechanism presumably as a result of differences of the polypeptide sequence at the N-terminal ATP-binding site of COX subunit IV. COX IV-2 is only marginally expressed in brain tissue and in astrocytes under physiological conditions. However, under hypoxic and toxic conditions, COX isoform IV-2 is up-regulated (Horvat et al. 2006; Singh et al. 2009).

This work was supported by the Deutsche Forschungsgemeinschaft (AR 343/1-3 and AR 343/4-1), the START-Program (S.A.) and IZKF BIOMAT (S.A., C.B.) of the Faculty of Medicine, RWTH Aachen University.

M. Misiak · S. Singh · S. Drewlo · C. Beyer · S. Arnold (✉)  
Institute for Neuroanatomy, Faculty of Medicine,  
RWTH Aachen University,  
Wendlingweg 2,  
52074 Aachen, Germany  
e-mail: sarnold@ukaachen.de

Cortical astrocytes exposed to hypoxia, i.e., conditions that are equivalent to depriving COX of its catalytic substrate, showed an up-regulation of COX IV-2. This in turn prevents the allosteric inhibition of COX by ATP and increases COX activity, irrespective of the ATP/ADP ratio, thereby suppressing the sensitivity of COX to high cellular energy levels (Arnold and Kadenbach 1997; Horvat et al. 2006). This was the first evidence for an oxygen concentration-dependent expression of mammalian COX subunit IV isoforms (Horvat et al. 2006).

Recently, we have reported a similar up-regulation of *cox4i2* transcripts after treatment of striatal astrocytes with 3-nitropropionic acid (NPA) for 48 h. The systemic application of NPA is a widely accepted in vitro model of Huntington's disease (HD). Interestingly, the NPA-mediated increase in necrotic cell death rate was not accompanied by decreased ATP levels but by an elevation of reactive oxygen species (ROS) production.

The most severely affected brain region in HD is the striatum (Brouillet et al. 1999; Vonsattel et al. 1985). However, other cerebral regions are also affected in HD patients, especially the cerebral cortex, although to a lesser extent (Albin 1995). With respect to a higher vulnerability of neural cells from striatum than from other brain regions, we have investigated COX isoform expression, mitochondrial peroxide production and astrocyte viability in striatum compared with cortex and mesencephalon. We have found brain region-specific differences with respect to the COX subunit IV isoform expression pattern, mitochondrially produced oxidative stress, and necrotic cell death.

## Materials and methods

### Materials

All chemicals were obtained from Roth (Karlsruhe, Germany), whereas reagents for molecular biological techniques and cell culture were purchased from Invitrogen (Karlsruhe, Germany), unless noted otherwise.

### Animals

BALB/c mice were purchased from Harlan Winkelmann GmbH (Borchen, Germany). All procedures were performed in strict accordance with the published welfare rules for the care and use of laboratory animals at the University Clinic Aachen and the Government of the State of North Rhine-Westphalia, Germany.

### Preparation of primary astrocyte cultures

Astroglial cultures were prepared from postnatal day 1 BALB/c mice as previously documented (Arnold et al.

2008). Briefly, brains from decapitated mice were removed and transferred into preparation buffer consisting of 10 mM HEPES, 154 mM NaCl, 10 mM glucose, 2 mM KCl, and 15  $\mu$ M bovine serum albumin. Cerebral striatum, cortex, and mesencephalon were dissected and, after removal of meninges, incubated in phosphate-buffered saline (PBS) containing 0.1% (v/v) trypsin and 0.02% (w/v) EDTA for 15 min. Subsequently, the tissue was minced with a Pasteur pipette and filtered through a 50  $\mu$ m nylon mesh. The cell suspension was centrifuged at 300g (Eppendorf, Hamburg, Germany) for 5 min. The cells were re-suspended in Dulbecco's modified Eagle's medium (DMEM; PAA, Coelbe, Germany) supplemented with 16% (v/v) fetal calf serum (PAA, Coelbe, Germany), 50 U/ml penicillin, 50  $\mu$ g/ml streptomycin, 0.25  $\mu$ g/ml amphotericin B (Fungizone), 2 mM L-glutamine (Glutamax) and plated onto poly-L-ornithine-coated (Sigma-Aldrich, Munich, Germany) culture dishes at a density of  $1\text{--}2 \times 10^6$  cells per  $\text{cm}^2$ . Astrocyte cultures were grown at 37°C in a humidified atmosphere of 95% air/5% CO<sub>2</sub>. Culture medium was replaced every third day. Before reaching confluence, cells were trypsinized and plated at lower density. Sub-confluent astrocytes were incubated in neurobasal medium (NBM) supplemented with 0.2% (v/v) B27, penicillin, streptomycin, Fungizone, and L-glutamine for 48 h and subsequently used for experiments.

### Cell treatment

Primary astrocyte cell cultures from the three different brain regions were placed on culture dishes at 37°C in a humidified atmosphere of 95% air/5% CO<sub>2</sub>. In the presence of NBM, cells were treated with NPA (Sigma-Aldrich, Munich, Germany) for the time indicated. Cells of the same preparation maintained under the same conditions except for NPA treatment served as controls.

### Small interfering RNA transfection

Transfection (lipofection) of cultured astrocytes with small interfering RNA (siRNA; Ambion, Huntingdon, UK) was carried out after the first passage of cells reached a confluence of approximately 85% and was incubated for 48 h in NBM containing 0.2% (v/v) B27 and 2 mM L-glutamine. To achieve the most efficient and least toxic knockdown of COX subunit isoform IV-2 in astrocytes, siRNA against *cox4i2* was applied (siRNA ID 175413; 5'-GCGAGUCAUGUGUCCCUtt-3') at a concentration of 20 nM. Oligonucleotides were mixed with 1.5  $\mu$ l Lipofectamine RNAiMAX (Invitrogen) in serum-free OptiMEM I (Invitrogen), incubated for 20 min, and added to the cells in antibiotics-free NBM. As a non-targeting siRNA control and for determination of transfection efficiency and

toxicity, silencer glyceraldehyde-3-phosphate dehydrogenase siRNA and siRNA negative control were used for transfection (Ambion). Transfection medium was changed to NBM with antibiotics after incubation for 24 h, and cells were kept for an additional 48 h in the presence or absence of 10 mM NPA. Transfection efficiencies of ca. 95% were reached in astrocytes with siRNA against *cox4i2* (data not shown).

#### Apoptosis and necrosis assays

To distinguish between apoptotic and necrotic astrocytes, siRNA-transfected, non-transfected, NPA-treated and untreated (control) cells were cultured on poly-L-ornithine-coated coverslips and stained with 3  $\mu$ M YO-PRO-1 (Invitrogen) for 30 min followed by the addition of 2  $\mu$ g/ml Hoechst 33342 trihydrochloride (Hoechst; Invitrogen) for 10 min under culturing conditions. Subsequently, cells were washed twice with PBS and fixed with approximately 100% (v/v) ice-cold methanol (Merck) for 10 min at  $-20^{\circ}\text{C}$ . Afterwards, cells were rinsed with PBS and incubated in  $2\times$  standard sodium citrate (SSC) buffer consisting of 0.3 M NaCl, 0.03 M sodium citrate, pH 7.0, for 20 min. Subsequently, cells were treated with 1  $\mu$ M propidium iodide (PI; Invitrogen) in  $2\times$  SSC buffer for 5 min followed by washing with PBS and mounting. Viable (Hoechst-positive), early apoptotic (Hoechst-, PI-positive), late apoptotic and necrotic (Hoechst-, YO-PRO-1-, and PI-positive) cell nuclei were scored under a fluorescence Axiophot microscope (Carl Zeiss, Oberkochen, Germany) at an excitation wavelength of 365 (Hoechst), 485 (YO-PRO-1), and 530 nm (PI). Early apoptotic cells showed a YO-PRO-1/PI-positive cytoplasm, whereas late apoptotic were distinguished from necrotic cells by their additional YO-PRO-1-, and PI-positive cytoplasm. Cell nuclei were counted in three separate experiments by counting cells in three distinct randomly selected areas per coverslip ( $3\times 10^5 \mu\text{m}^2$  per field) by using NIS-elements AR 3.0 software (Nikon, Düsseldorf, Germany).

#### Reverse transcription

Total RNA was isolated from treated and/or transfected cells and untreated controls by using PeqGold RNA pure (PeqLab, Erlangen, Germany) according to manufacturer's protocol. RNA concentration and purity were measured photometrically by using BioPhotometer (Eppendorf). RNA integrity was tested randomly by 1% (w/v) agarose denaturing gel electrophoresis and ethidium bromide staining and visualized under UV illumination. First strand complementary DNA (cDNA) was synthesized from 1  $\mu$ g total RNA. In brief, total RNA dissolved in 11  $\mu$ l diethyl pyrocarbonate (DEPC)-treated  $\text{H}_2\text{O}$  was pre-incubated at

$70^{\circ}\text{C}$  for 5 min and placed immediately on ice. Subsequently, the reaction buffer consisting of 10 U/ $\mu$ l MMLV reverse transcriptase, 10 mM dithiothreitol, 50 mM TRIS-HCl, pH 8.3, 75 mM KCl, 3 mM  $\text{MgCl}_2$ , 0.5 mM each dNTP (Roti-mixPCR3, Roth, Karlsruhe, Germany), and 15 ng/ $\mu$ l random primers was added to RNA giving a final volume of 20  $\mu$ l. After incubation for 40 min at  $55^{\circ}\text{C}$ , reverse transcription was stopped by heat-inactivating the enzyme at  $70^{\circ}\text{C}$  for 20 min. Addition of water instead of RNA served as a negative control. The gene 18 S ribosomal RNA (*18 S rRNA*) served for the normalization of samples, whereas the housekeeping gene hypoxanthine guanine phosphoribosyl transferase (*hprt*) spanning over intron-exon borders served as a control for RNA purity.

#### Quantitative real time polymerase chain reaction analysis

Gene transcription levels of COX subunit IV isoforms were measured by quantitative real time polymerase chain reaction (qRT-PCR) by using SYBR Green technology and were carried out on the iQ5 detection system (Bio-Rad, Munich, Germany). Forward and reverse primers for specific amplification of *cox4i1* (5'-TATGCTTCCCCACT TACGC-3' and 5'-GCCCACTGTCTTCCATT-3') and *cox4i2* (5'-AGATGAACCATCGCTCCAAC-3' and 5'-ATGGGGTTGCTTTCATGTC-3') were designed to eliminate the possibility of amplifying genomic DNA (Singh et al. 2009). After reverse transcription, a standard cDNA dilution series and sample cDNA diluted 1:10 were added to a solution containing 5  $\mu$ M primers and IQ SYBR Green Supermix (Bio-Rad) consisting of 25 U/ml iTaq polymerase, 50 mM KCl, 20 mM TRIS-HCl, 0.2 mM each dNTP, 3 mM  $\text{MgCl}_2$ , SYBR Green I, and stabilizers. The qRT-PCRs were conducted in standard 96-well plates and were composed of an initial denaturation step for 3 min at  $95^{\circ}\text{C}$  followed by 40 cycles consisting of 10 s at  $95^{\circ}\text{C}$ , 30 s at the appropriate annealing temperature for the target gene ( $60^{\circ}\text{C}$  for *cox4i1*, *18 S rRNA*;  $65^{\circ}\text{C}$  for *cox4i2*;  $61^{\circ}\text{C}$  for *hprt*), 30 s at  $72^{\circ}\text{C}$ , and 10 s at  $78^{\circ}\text{C}$ . To obtain melting curves for the resulting PCR products, a final step was added to the qRT-PCR consisting of 81 cycles of increasing temperature from  $55^{\circ}\text{C}$  to  $81^{\circ}\text{C}$  by  $0.5^{\circ}\text{C}$  for 10 s each step. The PCR products were quantified by using external standard dilution curves and the relative  $\Delta C_t$  (threshold cycle) method. Relative quantification relates the PCR signal of the target transcript to that of *18 S rRNA* in treated with respect to untreated cells. A test for an approximately equal efficiency of target amplification was performed by examining  $\Delta C_t$  value variations with template dilutions. *18 S rRNA* and *hprt* served as endogenous control in the validation experiments. The absolute value of the slope of log input amounts versus  $\Delta C_t$  should be approximately  $-3.3$ , with the efficiency being approximately 100%. The

validation experiments passed this test. The results are expressed as an average of triplicate samples of at least three independent experiments for control and treated cells.

#### Western blot analysis

Astrocytes were rinsed in PBS and subsequently lysed in ice-cold hypotonic RIPA buffer consisting of 50 mM TRIS-HCl, pH 7.4, 1 mM EDTA, 1% (v/v) Nonidet P-40 (Sigma, Igepal, CA, USA), and protease inhibitor cocktail (Complete Mini, Roche, Mannheim, Germany). After centrifugation for 20 min at 13,000g and 4°C, the supernatant was collected, and the protein concentration was measured by using the BCA Protein Assay Kit (Pierce, Rockford, Ill., USA). Protein samples (50 µg per lane) were loaded onto and separated by 12.5% (v/v) discontinuous sodium dodecyl sulphate-polyacrylamide gel electrophoresis and transferred onto a Hybond enhanced chemiluminescence (ECL) nitrocellulose membrane (Amersham Biosciences, Buckinghamshire, UK) by using the Trans-Blot Semi-Dry Electrophoretic Transfer Cell (Bio-Rad). An equal loading of samples and complete protein transfer were checked by the staining of blots and gels with Ponceau-S and Coomassie blue, respectively. Non-specific binding sites on the membrane were blocked by incubating it for 30 min in 5% (w/v) non-fat dry milk in TBST buffer consisting of 20 mM TRIS, pH 7.6, 150 mM NaCl, and 0.1% (v/v) Tween 20. The nitrocellulose membrane was then incubated for 24 h at 4°C with mouse anti-COX IV-1 antibody (MitoSciences, Eugene, OR, USA), mouse anti-COX IV-2 antibody (Abnova, Heidelberg, Germany), or rabbit anti-β-actin antibody (Sigma, USA) in TBST buffer containing 5% (w/v) non-fat dry milk. Detection was performed with horseradish peroxidase-conjugated goat anti-rabbit IgG (Sigma, USA) or rabbit anti-mouse antibody (Abcam, Cambridge, UK). Peroxidase activity was visualized by using the ECL method (Amersham Biosciences). For semi-quantitative evaluation of protein expression, immunoreactivity signals of protein bands were normalized to β-actin signals measured in the same blot.

#### ATP assay

The intracellular ATP content of cultured astrocytes was determined by using the ATP Bioluminescence Assay Kit HS II (Roche, Mannheim, Germany) according to the instructions of the manufacturer. In detail, NPA-treated and untreated (control) cells were washed with ice-cold PBS and re-suspended in an equal amount of cell lysis reagent and dilution buffer. After centrifugation for 10 min at 12,000g at 4°C (Eppendorf 5417R, Hamburg, Germany), supernatants were transferred into a microtiter plate (Dynex, West Sussex, UK), and an equal amount of

luciferase reagent was added. The luminescent reaction during absorbance/illumination at 562 nm was analyzed immediately in a microplate reader (Victor, 1420 Multilabel Counter, Perkin Wallac GmbH, Freiburg, Germany). The ATP content of the NPA-treated cells was calculated and normalized to the amount of proteins determined by applying the BCA Protein Assay Kit (Pierce, Bonn, Germany) with respect to untreated controls set as 100% (Singh et al. 2009).

#### Hydrogen peroxide detection

Peroxide generation was measured by using the Amplex Red Hydrogen Peroxide/Peroxidase Assay Kit (Invitrogen). Freshly isolated mitochondria from astrocytes (as described in detail in Singh et al. 2009) were resuspended in a minimal volume of mitochondrial buffer and added to 100 µl Krebs-Ringer phosphate buffer composed of 145 mM NaCl, 5.7 mM NaH<sub>2</sub>PO<sub>4</sub>, 4.86 mM KCl, 0.54 mM CaCl<sub>2</sub>, 1.22 mM MgSO<sub>4</sub>, 5.5 mM glucose, pH 7.35, containing 50 µM Amplex Red reagent and 0.1 U/ml horseradish peroxidase. Hydrogen peroxide in mitochondrial samples was detected by the formation of resorufin, the fluorescent oxidation product of Amplex Red, by using a fluorescence microplate reader (Tecan GENios, Crailsheim, Germany). The fluorescence of resorufin was excited at 535 nm, and its fluorescence emission was detected at 595 nm. Application of distinct H<sub>2</sub>O<sub>2</sub> concentrations (0–3 µM) served as a standard to quantify sample H<sub>2</sub>O<sub>2</sub> concentrations. Determination of the protein in mitochondria was used for normalization.

#### Statistical analysis

Data are presented as mean±SEM of at least three independent experiments (*n*). For statistical analysis, data were analyzed by applying an analysis of variance between groups followed by a post hoc two-tailed independent Student's *t* test by applying the software SPSS (Chicago, IL, USA). Values were regarded as statistically significant when compared with control (\*) and with NPA-treated samples (#) at \*\*\*/###*P*<0.001, \*\*/###*P*<0.01, \*/#*P*<0.05.

## Results

NPA treatment caused the highest vulnerability in astrocytes from striatum due to increased necrotic cell death rates

Isolated primary astrocytes from mouse brain striatum, cortex, and mesencephalon (postnatal day 1) showed cells which were mainly immunoreactive for the glial fibrillary acidic protein (>95%) and were virtually free of neurons,

oligodendrocytes, and microglial cells. To study brain region differences of astrocyte viability and mitochondrial characteristics in an in vitro model of HD, we treated primary astrocytes from striatum, cortex, and mesencephalon with 10 mM NPA for 48 h. Astrocytes were subsequently analyzed for cell viability, cytochrome c oxidase (COX) subunit IV isoform expression, intracellular ATP content, and mitochondrial peroxide production. To evaluate the specific role of COX isoform IV-2, astrocytes were additionally co-treated with NPA and siRNA against *cox4i2*.

Cell viability (Fig. 1a–d) was analyzed by different methods of labeling with the fluorescent indicator dyes Hoechst 33342 (Fig. 1b), YO-PRO-1 (Fig. 1c), and PI (Fig. 1d). Images of viable (arrows), early apoptotic (stars), late apoptotic (arrowheads), and necrotic cells (block arrows) are presented in Fig. 1a–d. The viable cells (Fig. 1a, arrow) showed an exclusive Hoechst-positive staining. Hoechst-staining of apoptotic bodies in cell nuclei combined with nuclear and cytoplasmic staining for PI (red), but an exclusive cytoplasmic YO-PRO-1-staining (green), was characteristic of early apoptotic cells (star). Late apoptotic (arrowhead) and necrotic (block arrow) cells showed Hoechst-, YO-PRO<sup>®</sup>-1-, and PI-positive nuclei. Late apoptotic were distinguished from necrotic astrocytes by an additional YO-PRO-1- and PI-positive staining of the cytoplasm. Based on the localization and appearance of the fluorescent dyes in cell nuclei and cytoplasm, necrotic (Fig. 1e) and apoptotic cells (Fig. 1f) were counted and calculated as a percentage of the total cell number. Cultured astrocytes from all three brain regions showed a higher degree of necrotic than apoptotic cell death rates. Striatal astrocytes demonstrated the highest necrotic cell death rate in comparison with cortical and mesencephalic cells (Fig. 1e). Taking the basal level of necrotic cell death rates in untreated astrocytes into account, NPA treatment caused approximately six-, two-, and three-fold increases in striatal, cortical, and mesencephalic cells, respectively. After NPA treatment, the apoptosis rates (Fig. 1f) were increased by approximately 100%, 50%, and 250% in striatal, cortical, and mesencephalic astroglia, respectively. Necrotic and apoptotic cell death rates occurred in astrocytes with the same differences between the three different brain regions, only to a lesser degree when NPA was applied for shorter incubation times. A siRNA-mediated knockdown of *cox4i2* transcripts decreased necrotic cell death significantly in astrocytes from all three brain regions (Fig. 1e) but increased the apoptotic cell death rate (Fig. 1f) in striatal and mesencephalic cells by approximately four- and two-fold, respectively. An increase of apoptotic cell death rates without exerting any effect on necrotic cell death rates was also observed after application of a siRNA against *cox4i2* in the absence of NPA, but not after incubation with negative siRNA (data not shown).

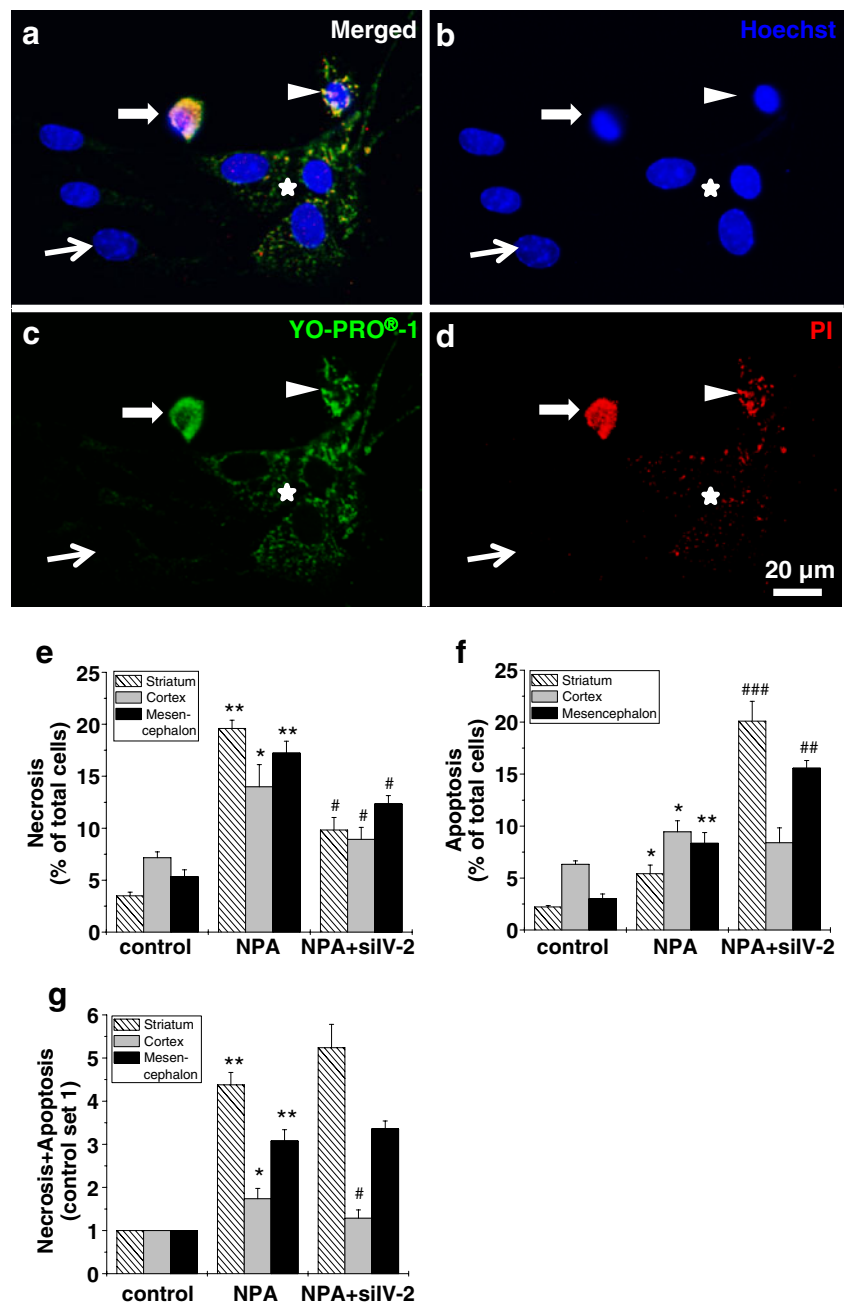
These increased apoptotic cell death rates occurred in striatal and mesencephalic, but not in cortical astrocyte cultures and could account for the increased apoptosis rates when NPA and siRNA against *cox4i2* were co-applied (Fig. 1f). The NPA-mediated overall cell death rates (Fig. 1g) were highest in striatal astrocytes followed by mesencephalic and cortical astrocytes. Due to the effect of siRNA against *cox4i2* on apoptosis in astrocytes from striatum and mesencephalon, the co-treatment of astrocytes with NPA and siRNA against *cox4i2* failed to decrease overall cell death in striatal and mesencephalic astroglia.

COX subunit IV isoform transcription and protein expression was affected by NPA in a brain region-specific manner

Astrocytes from all three brain regions showed, under normal culturing conditions, a predominance of *cox4i1* transcription (Fig. 2a), whereas *cox4i2* was only marginally transcribed (Fig. 2b). Treatment of cultured astrocytes from striatum, cortex, and mesencephalon with 10 mM NPA for 48 h revealed an elevation of *cox4i2* transcript levels of approximately four-, eight-, and four-fold, respectively (Fig. 2b). The NPA-mediated increased *cox4i2* transcript levels were decreased to basal levels by co-application of siRNA against *cox4i2*. After NPA treatment, the transcription levels of *cox4i1* were decreased in striatal astrocytes by approximately 50%, were elevated in cortical astroglia by approximately 40%, and remained unchanged in mesencephalic cells as a result of the NPA treatment (Fig. 2a). A siRNA against *cox4i2* exerted no significant effect on the *cox4i1* transcription levels (data not shown), except that the application of siRNA in the presence of NPA caused, in comparison with samples treated with NPA only, a decrease in *cox4i1* transcript levels in cortical astrocytes (Fig. 2a). The differentially regulated *cox4i2* and *cox4i1* transcript levels are summarized in the presentation of the *cox4i2/cox4i1* ratio (Fig. 2c). The highest NPA-mediated up-regulation of the *cox4i2/cox4i1* ratio was observed for striatal astrocytes followed by cortical and mesencephalic astrocytes. The co-treatment of astrocytes from all three brain regions with siRNA against *cox4i2* completely reverted the NPA-mediated increased *cox4i2/cox4i1* ratio.

The changes in the transcription levels of the COX subunit IV isoforms were mostly reflected by concomitant changes in the protein levels of the COX isoforms (Fig. 3). COX IV-1 and COX IV-2 protein levels were normalized to  $\beta$ -actin (Fig. 3a). COX isoform IV-1 was the predominant COX subunit IV isoform expressed under normal culturing conditions in astrocytes from all three brain regions (Fig. 3a). The NPA-mediated transcriptional increase of *cox4i2* and the changes of *cox4i1* were also observed at the protein level, when the optical densities of Western blot

**Fig. 1** Astrocytes from striatum showed the highest vulnerability after NPA treatment when compared with astroglia from cortex and mesencephalon. **a–d** Astrocytes stained with fluorescent viability indicator dyes are presented in a merged picture (**a**) of Hoechst-stained (**b**), YO-PRO-1-stained (**c**), and PI-stained (**d**) cells. Viable (*arrow*; Hoechst-positive), early apoptotic (*star*; Hoechst-, PI-positive), late apoptotic (*arrowhead*), and necrotic (*block arrow*; Hoechst-, YO-PRO-1-, and PI-positive) fluorescent cell nuclei are indicated. Early apoptotic cells showed a YO-PRO-1-/PI-positive cytoplasm. Late apoptotic were distinguished from necrotic cells by their additional YO-PRO-1- and PI-positive cytoplasm. **e–g** Astrocytes from striatum (*striped columns*), cortex (*gray columns*), and mesencephalon (*black columns*) were untreated (*control*), NPA-treated (*NPA*), or co-treated with NPA and siRNA against *cox4i2* (*NPA+siIV-2*). Necrotic (**e**), apoptotic (**f**), and overall cell death (**g**; *control set 1*) was assessed by counting astrocytes stained with the appropriate fluorescent viability indicator dyes. Data represent mean $\pm$ SEM (\* $\#P<0.05$ , \*\* $\#\#P<0.01$ ,  $\#\#\#P<0.001$ ,  $n=8$ ) of samples as compared with control ( $\bar{\phantom{0}}$ ) and with NPA-treated cells ( $\#$ )



bands were calculated and compared with control protein levels set 100% (Fig. 3). Western blot results showed a COX IV-2 up-regulation upon NPA treatment by approximately three-fold in striatal (Fig. 3b) and cortical (Fig. 3c) astrocytes and by 50% in mesencephalic (Fig. 3d) astrocytes. COX IV-1 protein content was down-regulated upon NPA exposure in striatal astrocytes to approximately 40% of control levels (Fig. 3b), whereas it was up-regulated by approximately two-fold in cortical astroglia (Fig. 3c) and remained unchanged in mesencephalic cells (Fig. 3d). Accordingly, the COX IV-2/COX IV-1 ratio demonstrated the highest increase by 14-fold in striatal astroglia, whereas

cortical and mesencephalic cells exhibited an increase by 170% and 45%, respectively (Fig. 3e). A siRNA-mediated knockdown of NPA-induced increases of COX IV-2 efficiently decreased the appropriate protein levels but did not affect COX IV-1 protein expression levels when compared with control levels in astrocytes from all brain regions. However, NPA-mediated decreased COX IV-1 protein levels in striatal astrocytes were increased by co-application of a siRNA against *cox4i2* to control levels, up-regulated COX IV-1 protein levels in cortical cells were decreased by siRNA, and COX IV-1 levels in mesencephalic astrocytes remained unchanged.

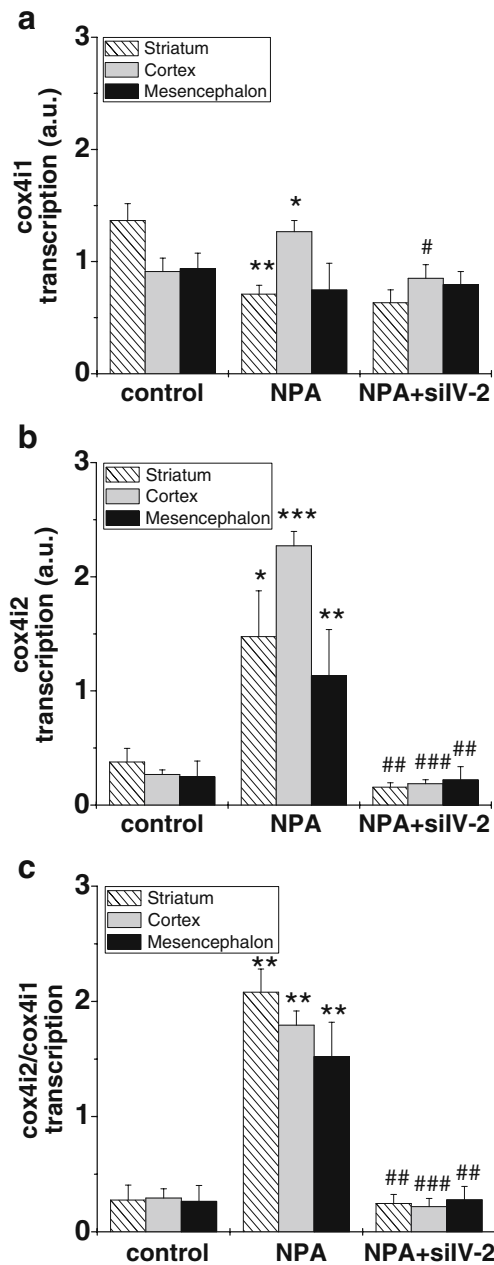


**Fig. 2** Transcript ratio of *cox4i2* to *cox4i1* is increased in striatal astrocytes to the highest degree based on an up-regulation of *cox4i2* and a down-regulation of *cox4i1*. Astrocytes from striatum (*striped columns*), cortex (*gray columns*), and mesencephalon (*black columns*) were untreated (*control*), NPA-treated (*NPA*), or co-treated with NPA and siRNA against *cox4i2* (*NPA+siIV-2*). Quantitative real-time polymerase chain reaction revealed differently regulated *cox4i1* (a) and up-regulated *cox4i2* transcript levels (b) by NPA; this was also reflected in the *cox4i2/cox4i1* transcript level ratio (c) in astrocytes from three brain regions (\*). A siRNA against *cox4i2* decreased *cox4i2* transcript levels, whereas *cox4i1* was not significantly affected except for decreased levels in cortical astrocytes when compared with NPA-treated samples (#). Data represent mean±SEM (\* $P<0.05$ , \*\*/### $P<0.01$ , \*\*\*/#### $P<0.001$ ,  $n=5$ )

NPA caused an elevation of intracellular ATP content and mitochondrial peroxide production in astrocytes from all three brain regions, but to a different extent

Treatment of astrocytes from all brain regions caused an up-regulation of intracellular ATP levels (Fig. 4a). The highest elevation of the ATP content (by three-fold) was detected in cortical astrocytes, whereas striatal and mesencephalic astroglia exhibited an increase by approximately 20% and 40%, respectively. A COX IV-2 knockdown revealed a diminished ATP elevation upon NPA treatment by 10% and 90% in striatal and cortical astroglia, respectively, whereas it was further up-regulated by 70% in mesencephalic cells.

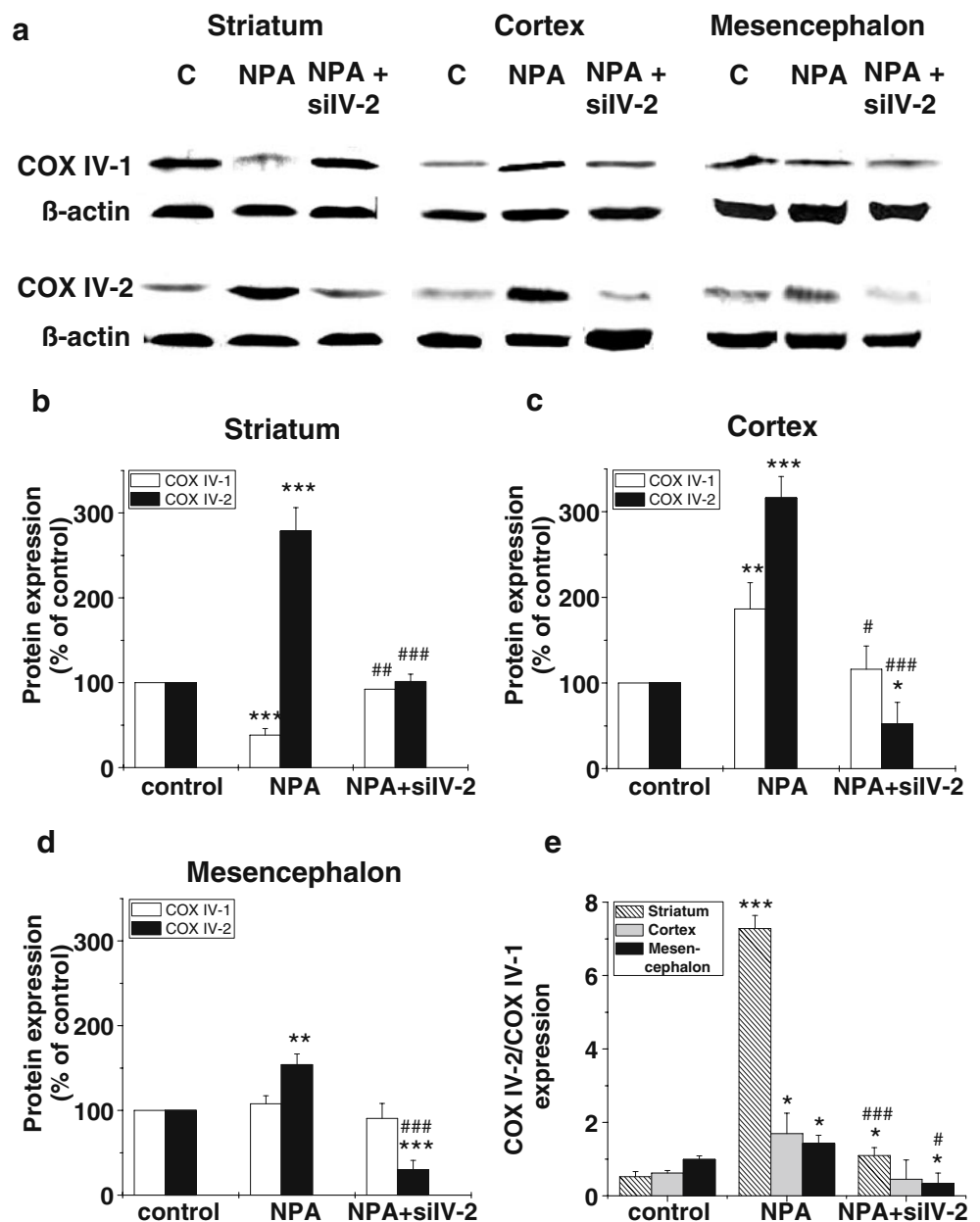
The peroxide production was measured as an indicator of increased oxidative stress caused by mitochondria (Fig. 4b). We observed, in astrocytes from all three brain regions, an elevated mitochondrial peroxide production, which was the highest (by 700%) in striatal astrocytes, whereas an increase by 140% and 135% were measured for cortical and mesencephalic astroglia, respectively. The NPA-mediated elevation of peroxide production was decreased due to a parallel COX IV-2 knockdown by 300%, 65%, and 75% in striatal, cortical, and mesencephalic astrocytes, respectively.

## Discussion

Genetic mutations, transcriptional dysregulation, excitotoxicity, protein aggregation, mitochondrial dysfunction, selective neuronal vulnerability, oxidative stress, and apoptosis are common to multiple neurodegenerative diseases, such as HD (Kumar et al. 2010). In our recently published study (Singh et al. 2009), we examined the role of mitochondrial structural and functional characteristics of striatal astrocytes in NPA-mediated toxicity. We chose striatal astrocytes for this in vitro model of HD with respect to the selective loss of striatal astrocytes after systemic application of NPA (Nishino et al. 1995). Here, we aimed to demonstrate striatum-specific NPA-mediated effects on astrocyte viability in comparison with cortex and mesencephalon.

The cause of neurodegeneration in HD is apparently multifactorial (Cattaneo et al. 2001). A number of “initiator” mechanisms have been suggested and include abnormal interactions between mutated huntingtin and neuronal proteins (Cattaneo et al. 2001; Gervais et al. 2002; Subramaniam et al. 2009), transcriptional dysregulations (Cha 2000; Zuccato et al. 2001), mitochondrial defects and oxidative damage (Arnold and Beyer 2009; Beal 2000; Browne et al. 1997; Panov et al. 2002; Sawa et al. 1999), and indirect activation of the excitotoxic cascade leading to apoptosis (Ona et al. 1999; Sanchez et al. 1999; Saudou et al. 1998) or necrosis (Brouillet et al. 1999; Singh et al. 2009). Recently,

**Fig. 3** COX IV-1 and COX IV-2 protein expression supports the transcription data of NPA-induced up-regulation of *cox4i2*. Astrocytes from striatum, cortex, and mesencephalon were untreated (C or control), NPA-treated (NPA), or co-treated with NPA and siRNA against *cox4i2* (NPA+siIV-2). **a** Western blots. **b–d** Calculations of optical densities of Western blot bands of COX IV-1 (white columns) and COX IV-2 (black columns) normalized to  $\beta$ -actin protein levels and in comparison with COX isoform levels under control conditions set 100%. **b** Striatum. **c** Cortex. **d** Mesencephalon. **e** Ratios of COX IV-2/COX IV-1 protein levels are presented for astrocytes from striatum (striped columns), cortex (gray columns), and mesencephalon (black columns) relative to control set 1. **b–e** Data represent mean $\pm$ SEM (\* $P$ <0.05, \*\* $P$ <0.01, \*\*\* $P$ <0.001,  $n$ =4) and siRNA+NPA co-treated samples compared with NPA-treated samples (#)



Subramaniam and colleagues have provided a possible explanation for the striatum being preferentially involved in HD by studying Rhes, an interaction partner protein of mutated huntingtin (Subramaniam et al. 2009).

In support of the hypothesis that mitochondrial defects might play a role in HD pathogenesis (Beal 2000; Blum et al. 2003), intoxication with the succinate dehydrogenase (SDH) inhibitor NPA in rats and non-human primates produces abnormal movements, cognitive deficits, and striatal degeneration (Beal 2000; Blum et al. 2001, 2002; Brouillet et al. 1995). Despite the preferential vulnerability of the striatum to NPA toxicity, cell loss in certain areas of the cerebral cortex anatomically connected to the striatum has also been observed several weeks after the onset of striatal degeneration

(Mittoux et al. 2002). However, brain region-specific differences are not related to a differential effect of NPA on SDH activity because the latter is similarly inhibited by NPA in striatal and cortical neurons (Galas et al. 2004). We have therefore focused on the role of COX subunit IV isoform expression in energy production, mitochondrially caused oxidative stress, and astrocyte vulnerability in striatum compared with cortex and mesencephalon.

NPA as an inhibitor of SDH, which is complex II of the mitochondrial respiratory chain, impairs mitochondrial energy production (Ayala et al. 2007; Beal 2005; Gu et al. 1996; Schapira 1997). Although we have detected an increase in the vulnerability of mainly striatal astrocytes when compared with cortical and mesencephalic astrocytes,



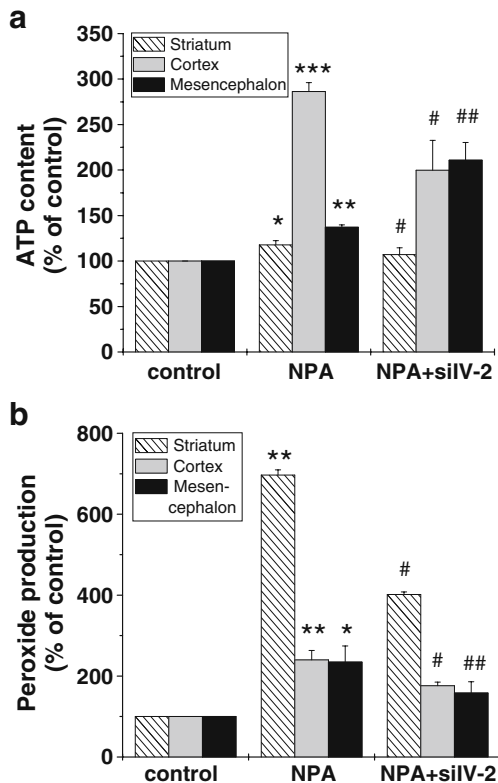


**Fig. 4** Intracellular ATP content and peroxide production exhibited highest levels for cortex and striatum, respectively. Astrocytes from striatum (*striped columns*), cortex (*gray columns*), and mesencephalon (*black columns*) were untreated (*control*), NPA-treated (*NPA*), or co-treated with NPA and siRNA against *cox4i2* (*NPA+siIV-2*). The values of ATP content and peroxide production were calculated relative to control (\*) set 100%, compared with NPA-treated samples (#) and represent mean±SEM (\*# $P$ <0.05, \*\*/### $P$ <0.01, \*\*\* $P$ <0.001,  $n$ =6)

this is apparently not attributable to a diminished ATP content, but rather to an elevated peroxide production by astrocytic mitochondria. Oxidative damage and metabolic dysfunction have been implicated in HD (Browne et al. 1997). The peroxide levels in striatal astrocytes exceeded those in cortical and mesencephalic cells by several fold. Surprisingly, the impaired astrocyte viability is paralleled by increased, instead of the expected decreased, intracellular ATP levels, which were highest in cortical astrocytes and lowest in striatal astrocytes. This apparently reflects the overall cell death rate in NPA-treated astrocytes, which was the lowest in cortical astrocytes and highest in striatal astrocytes. A maintained oxidative energy production by the respiratory chain during complex II inhibition can, at least in part, be explained by electron entry via complex I of the mitochondrial respiratory chain. In support of this, a study by Folbergrová and colleagues has demonstrated that complex I inhibition was not accompanied by impaired ATP production, which is apparently attributable to excess capacity of complex I as documented by energy thresholds (Folbergrová et al. 2009). Thus, elevated ROS production

seems to be the major reason for NPA-mediated cell death in striatal astrocytes. The lowest ATP level together with the highest peroxide production in striatal astrocytes might explain the highest level of necrotic cell death rates being seen in astrocyte cultures from striatum when compared with cortex or mesencephalon.

NPA-mediated elevated overall cell death rates of striatal astrocytes were caused by necrosis rather than by apoptosis. This observation of higher necrotic than apoptotic cell death rates supports our earlier report on striatal astroglia (Singh et al. 2009) and has been observed in astrocytes of all three brain regions, although to a different extent. Increased necrosis rates were accompanied by increased COX IV-2 and decreased COX IV-1 protein levels preceded by an up-regulation of *cox4i2* and down-regulation of *cox4i1* transcript levels, specifically in striatal astrocytes. COX isoform IV-1 is the predominant isoform in astrocytes from all three brain regions under normal culturing conditions. *Cox4i1* transcripts are exchanged for *cox4i2* under hypoxic and toxic conditions (Horvat et al. 2006; Singh et al. 2009). However, protein levels are more important for the functional consequences of enzyme activities than are transcript levels. Furthermore, not only the absolute COX isoform IV-2 levels are valuable, but also those of COX IV-1. Therefore, we have calculated the COX IV-2/COX IV-1 protein ratio in NPA-treated astrocytes and found the most prominent elevation of COX IV-2/COX IV-1 in striatal astrocytes accompanied by the highest peroxide production and necrotic cell death rate. Cortical and mesencephalic cells exhibited a much lower COX IV-2/COX IV-1 ratio attributable to up-regulated or constant COX IV-1 additional to the increased COX IV-2 levels, respectively. This might be one of the reasons for a partial protection of astrocytes from other brain regions than the striatum. A knockdown specific for COX IV-2 achieved by applying siRNA against this COX isoform caused a down-regulation of necrotic cell death rates in all three brain regions indicating a causal relationship between the expression pattern of the COX subunit IV isoform and mitochondrial peroxide production and necrotic cell death.

Knockdown of COX IV-2 in the presence of the mitochondrial toxin NPA reverted necrotic cell death, but induced an elevation of apoptotic cell death rates in striatal and mesencephalic astrocytes, but not in cortical astrocytes. This does not occur when a negative unspecific siRNA was applied (data not shown). However, the application of siRNA against *cox4i2* in the absence of NPA also caused increased apoptosis rates without exerting any effect on necrotic cell death rates (data not shown). These siRNA-mediated increased apoptotic cell death rates occurred in striatal and mesencephalic astrocyte cultures, but not in cortical astrocyte cultures, and might account for the increased apoptosis rates when NPA and siRNA against

*cox4i2* were co-applied. Transfection of untreated and NPA-treated astrocytes with siRNA against one of the COX subunit IV isoforms did affect neither the transcription nor the protein expression levels of the other isoform (data not shown). Elevated apoptosis rates are, therefore, apparently a specific feature of COX IV-2 knockdown in untreated and NPA-treated astrocytes from striatum and mesencephalon, two highly vulnerable brain regions. Interestingly, the cortex was the only brain region in which astrocytes showed an NPA-mediated up-regulation of COX IV-1 protein levels. This indicates a role of increased COX IV-1 levels under toxic conditions in protecting cells from undergoing apoptosis.

Interestingly, a switch from *cox4i1* to *cox4i2* transcription is accompanied by increased catalytic activity of COX (Singh et al. 2009). This, in turn, might serve as an explanation of the increased intracellular ATP content in our experiments. Most of the respiratory chain complexes exhibit a higher capacity than the activity that they show under physiological conditions. The lowest excess capacity has been proposed for COX, thus being the rate-limiting enzyme of the respiratory chain (Villani et al. 1998). COX is the sole enzyme of the respiratory chain known to be regulated by allosteric factors, such as ATP binding in exchange for ADP to the inner mitochondrial domain of COX subunit IV-1 (Arnold and Kadenbach 1997, 1999; Kadenbach and Arnold 1999). This enables the enzyme to detect the ATP level and to adjust COX and thus respiratory chain activity to energy demand (Arnold and Kadenbach 1997; Horvat et al. 2006; Singh et al. 2009). The expression of nuclear-encoded subunit isoforms provides a basis for the fine-tuning of COX activity in response to specific metabolic needs in different cell types and tissues. Previously, we have shown a cell type-specific expression of COX subunit IV isoforms in the brain (Horvat et al. 2006). Thus, the ubiquitously and highly expressed COX isoform IV-1 renders astrocytes able to detect neuronal energy demand and to adjust oxidative energy metabolism to provide neurons with the energy substrate lactate according to the neuron-glia metabolic cooperation (Pellerin 2003). However, under hypoxic and toxic conditions, COX isoform IV-2 is up-regulated in astrocytes (Horvat et al. 2006; Singh et al. 2009). This isoform exhibits a higher catalytic activity than COX IV-1 at the expense of an abolished sensitivity of the enzyme towards the cellular energy level (Horvat et al. 2006; Singh et al. 2009). Another consequence of COX IV-2 expression is elevated mitochondria-produced oxidative stress (Singh et al. 2009). This observation has also been made for NPA-treated astrocytes from cortex and mesencephalon, but to a much lower extent. We correlate this to the lower COX subunit IV isoform ratio in astroglia from these two brain regions compared with the striatum. Preliminary data on the three

different brain regions of a HD mouse model indicate the existence of a COX IV isoform-mediated mitochondrial mechanism of selective striatal vulnerability in vivo and will be subject of our future studies.

In conclusion, we have found that COX subunit IV isoforms play an essential brain region-specific role in mitochondrial energy metabolism, oxidative stress, and consequently survival of astrocytes under toxic conditions. NPA-treated astrocytes from the striatum showed a higher vulnerability than those from the cortex and mesencephalon. This provides additional mechanistic insights into the brain region-specific role of COX and mitochondria in cell viability under toxic conditions. Our observations support the concept of a selective vulnerability of the striatum in HD.

**Acknowledgements** We thank Petra Ibold for excellent technical assistance and Sascha Drewlo for helpful technical support.

## References

- Albin RL (1995) Selective neurodegeneration in Huntington's disease. *Ann Neurol* 38:835–836
- Arnold S, Beyer C (2009) Neuroprotection by estrogen in the brain: the mitochondrial compartment as presumed therapeutic target. *J Neurochem* 110:1–11
- Arnold S, Kadenbach B (1997) Cell respiration is controlled by ATP, an allosteric inhibitor of cytochrome-c oxidase. *Eur J Biochem* 249:350–354
- Arnold S, Kadenbach B (1999) The intramitochondrial ATP/ADP-ratio controls cytochrome c oxidase activity allosterically. *FEBS Lett* 443:105–108
- Arnold S, Araújo GW de, Beyer C (2008) Gender-specific regulation of mitochondrial fusion and fission gene transcription and viability of cortical astrocytes by steroid hormones. *J Mol Endocrinol* 41:289–300
- Ayala A, Venero JL, Cano J, Machado A (2007) Mitochondrial toxins and neurodegenerative diseases. *Front Biosci* 12:986–1007
- Beal MF (2000) Energetics in the pathogenesis of neurodegenerative diseases. *Trends Neurosci* 23:298–304
- Beal MF (2005) Mitochondria take center stage in aging and neurodegeneration. *Ann Neurol* 58:495–505
- Blum D, Gall D, Cuvelier L, Schiffmann SN (2001) Topological analysis of striatal lesions induced by 3-nitropropionic acid in the Lewis rat. *Neuroreport* 12:1769–1772
- Blum D, Galas MC, Gall D, Cuvelier L, Schiffmann SN (2002) Striatal and cortical neurochemical changes induced by chronic metabolic compromise in the 3-nitropropionic model of Huntington's disease. *Neurobiol Dis* 10:410–426
- Blum D, Hourez R, Galas MC, Popoli P, Schiffmann SN (2003) Adenosine receptors and Huntington's disease: implications for pathogenesis and therapeutics. *Lancet Neurol* 2:366–374
- Brouillet E, Hantraye P, Ferrante RJ, Dolan R, Leroy-Willig A, Kowall NW, Beal MF (1995) Chronic mitochondrial energy impairment produces selective striatal degeneration and abnormal choreiform movements in primates. *Proc Natl Acad Sci USA* 92:7105–7109
- Brouillet E, Condé F, Beal MF, Hantraye P (1999) Replicating Huntington's disease phenotype in experimental animals. *Prog Neurobiol* 59:427–468

- Browne SE, Bowling AC, MacGarvey U, Baik MJ, Berger SC, Muqit MM, Bird ED, Beal MF (1997) Oxidative damage and metabolic dysfunction in Huntington's disease: selective vulnerability of the basal ganglia. *Ann Neurol* 41:646–653
- Cattaneo E, Rigamonti D, Goffredo D, Zuccato C, Squitieri F, Sipione S (2001) Loss of normal huntingtin function: new developments in Huntington's disease research. *Trends Neurosci* 24:182–188
- Cha JH (2000) Transcriptional dysregulation in Huntington's disease. *Trends Neurosci* 23:387–392
- Folbergrová J, Ješina P, Haugvicová R, Lisý V, Houštěk J (2009) Sustained deficiency of mitochondrial complex I activity during long periods of survival after seizures induced in immature rats by homocysteic acid. *Neurochem Int* 56:394–403
- Galas MC, Bizat N, Cuvelier L, Bantubungi K, Brouillet E, Schiffmann SN, Blum D (2004) Death of cortical and striatal neurons induced by mitochondrial defect involves differential molecular mechanisms. *Neurobiol Dis* 15:152–159
- Gervais FG, Singaraja R, Xanthoudakis S, Gutekunst CA, Leavitt BR, Metzler M, Hackam AS, Tam J, Vaillancourt JP, Houtzager V, Rasper DM, Roy S, Hayden MR, Nicholson DW (2002) Recruitment and activation of caspase-8 by the Huntingtin-interacting protein Hip-1 and a novel partner Hippi. *Nat Cell Biol* 4:95–105
- Grossman LI, Lomax MI (1997) Nuclear genes for cytochrome c oxidase. *Biochim Biophys Acta* 1352:174–192
- Gu M, Gash MT, Mann VM, Javoy-Agid F, Cooper JM, Schapira AH (1996) Mitochondrial defect in Huntington's disease caudate nucleus. *Ann Neurol* 39:385–389
- Horvat S, Beyer C, Arnold S (2006) Effect of hypoxia on the transcription pattern of subunit isoforms and the kinetics of cytochrome c oxidase in cortical astrocytes and cerebellar neurons. *J Neurochem* 99:937–951
- Kadenbach B, Arnold S (1999) A second mechanism of respiratory control. *FEBS Lett* 447:131–134
- Kadenbach B, Hüttemann M, Arnold S, Lee I, Bender E (2000) Mitochondrial energy metabolism is regulated via nuclear-coded subunits of cytochrome c oxidase. *Free Radic Biol Med* 29:211–221
- Kadenbach B, Arnold S, Lee I, Hüttemann M (2004) The possible role of cytochrome c oxidase in stress-induced apoptosis and degenerative diseases. *Biochim Biophys Acta* 1655:400–408
- Kumar P, Kalonia H, Kumar A (2010) Huntington's disease: pathogenesis to animal models. *Pharmacol Rep* 62:1–14
- Mittoux V, Ouary S, Monville C, Lisovoski F, Poyot T, Conde F, Escartin C, Robichon R, Brouillet E, Peschanski M, Hantraye P (2002) Corticostriatal pallidal neuroprotection by adenovirus-mediated ciliary neurotrophic factor gene transfer in a rat model of progressive striatal degeneration. *J Neurosci* 22:4478–4486
- Nishino H, Shimano Y, Kumazaki M, Sakurai T (1995) Chronically administered 3-nitropropionic acid induces striatal lesion attributed to dysfunction of the blood-brain barrier. *Neurosci Lett* 186:161–164
- Ona VO, Li M, Vonsattel JP, Andrews LJ, Khan SQ, Chung WM, Frey AS, Menon AS, Li XJ, Stieg PE, Yuan J, Penney JB, Young AB, Cha JH, Friedlander RM (1999) Inhibition of caspase-1 slows disease progression in a mouse model of Huntington's disease. *Nature* 399:263–267
- Panov AV, Gutekunst CA, Leavitt BR, Hayden MR, Burke JR, Strittmatter WJ, Greenamyre JT (2002) Early mitochondrial calcium defects in Huntington's disease are a direct effect of polyglutamines. *Nat Neurosci* 5:731–736
- Pellerin L (2003) Lactate as a pivotal element in neuron-glia metabolic cooperation. *Neurochem Int* 43:331–338
- Sanchez I, Xu CJ, Juo P, Kakizaka A, Blenis J, Yuan J (1999) Caspase-8 is required for cell death induced by expanded polyglutamine repeats. *Neuron* 22:623–633
- Saudou F, Finkbeiner S, Devys D, Greenberg ME (1998) Huntingtin acts in the nucleus to induce apoptosis but death does not correlate with the formation of intranuclear inclusions. *Cell* 95:55–66
- Sawa A, Wiegand GW, Cooper J, Margolis RL, Sharp AH, Lawler JF Jr, Greenamyre JT, Snyder SH, Ross CA (1999) Increased apoptosis of Huntington disease lymphoblasts associated with repeat length-dependent mitochondrial depolarization. *Nat Med* 5:1194–1198
- Schapira AH (1997) Mitochondrial function in Huntington's disease: clues for pathogenesis and prospects for treatment. *Ann Neurol* 41:141–142
- Singh S, Misiak M, Beyer C, Arnold S (2009) Cytochrome c oxidase isoform IV-2 is involved in 3-nitropropionic acid-induced toxicity in striatal astrocytes. *Glia* 57:1480–1491
- Subramaniam S, Sixt KM, Barrow R, Snyder SH (2009) Rhes, a striatal specific protein, mediates mutant-huntingtin cytotoxicity. *Science* 324:1327–1330
- Tsukihara T, Aoyama H, Yamashita E, Tomizaki T, Yamaguchi H, Shinzawa-Itoh K, Nakashima R, Yaono R, Yoshikawa S (1996) The whole structure of the 13-subunit oxidized cytochrome c oxidase at 2.8 Å. *Science* 272:1136–1144
- Villani G, Greco M, Papa S, Attardi G (1998) Low reserve of cytochrome c oxidase capacity in vivo in the respiratory chain of a variety of human cell types. *J Biol Chem* 273:31829–31836
- Vonsattel JP, Myers RH, Stevens TJ, Ferrante RJ, Bird ED, Richardson EP Jr (1985) Neuropathological classification of Huntington's disease. *J Neuropathol Exp Neurol* 44:559–577
- Zuccato C, Ciammola A, Rigamonti D, Leavitt BR, Goffredo D, Conti L, MacDonald ME, Friedlander RM, Silani V, Hayden MR, Timmusk T, Sipione S, Cattaneo E (2001) Loss of huntingtin mediated BDNF gene transcription in Huntington's disease. *Science* 293:493–498